Computational Mechanics 16 (1995) 273–280 © Springer-Verlag 1995

Multiple-cracked fatigue crack growth by BEM

A. M. Yan, H. Nguyen-Dang

Abstract The dual boundary element method is applied for the two-dimensional linear elastic analysis of fatigue problem of multiple-cracked body. The traction integral equation is applied on ones of surfaces of cracks while the usual displacement integral equation simultaneously on the others. General multiple crack growth problem is solved in a single-region formulation. All crack surfaces are discretized with discontinuous quadratic boundary elements. J-integral technique is used to evaluate stress intensity factors. The real extension path of cracks is simulated by a linear incremental crack extension, based on the maximum principal stress criterion. For each increment analysis of the cracks, crack extension is conveniently modelled with new boundary elements. Remeshing is no longer necessary. Fatigue life analysis is carried out with Paris' formulae. Several numerical examples show high efficiency of present method.

1 Introduction

Investigation and description of fatigue crack growth are essential if the reliability of structures under cyclic loading is to be ensured. Cracks, as a result of manufacturing fabrication defects or localised damage in service, may extend under the condition of service leading to a decrease of the structure strength and finally fracture failure of the structure. In linear elastic fracture mechanics, one uses the stress intensity factors as a fundamental parameter, which determine solely the stress field in the neighbourhood of crack-tip and control the propagation of cracks. For each increment of the crack extension, a stress analysis is carried out and the stress intensity factors are evaluated. Because of the irregulation and complexity of boundary geometry of realistic problems, efficient numerical techniques become necessary.

The boundary element method (BEM) has been successfully applied to the analysis of cracked bodies. However, because the coincidence of the crack surfaces rises to a singular system of algebraic equations, the solution of general crack problems cannot be achieved with the direct application of the BEM in a single region analysis. Some special techniques have been devised to overcome this difficulty. Among them, the dual boundary element method (DBEM) drew recently great intention: Bueckner (1973), Watson (1986), Hong and Chen (1988). Its effective implement is realised by Portela, Aliabadi and Rooke (1991). Recently, a development of application of the DBEM to a multiple-cracked body has been achieved by Yan and Nguyen-Dang (1994 a, b). Simulation of fatigue growth of cracks by classical finite element method (FEM) is generally in high cost, because the finite element mesh has to be recreated after each extension of crack. To overcome this difficulty, the FEAM (Finite Element Alternating Method) has been proposed, Park, J. H. et al. (1993, 1994), where FEM is only used for a uncracked structure to obtain the traction in position of crack while an analytical method is used for the solution of fracture parameters and no remeshing is needed in simulating the crack growth phenomena. The present dual boundary element method may be considered as alternative. In fact, crack extension is conveniently modelled with new boundary elements for each increment analysis of the cracks and again remeshing is also not necessary.

In this paper, the dual boundary element method is applied to study fatigue crack propagation and life evaluation. The principal objective of this research concerns on the multiple-cracked body. In fact, the multiple crack fatigue problems, especially the interaction and propagation tendency of multiple cracks catch the attention of scientists. The real extension path of cracks is simulated by an incremental crack-extension, that is to assume a piece-wise linear discretization of crack extension path. The maximum principle stress criterion is applied to predict the direction of crack extension. Fatigue life evaluation is based on Paris' law. Numerical examples are illustrated to point out the efficiency of the present method.

2 Dual boundary element method

Dual boundary element method is based on the displacement and traction boundary integral equations. In the absence of body force, the boundary integral representation of the displacement components u_i at an internal point y for a domain S with a boundary Γ is:

$$u_i(y) = \int_\Gamma U_{ij}(y,x)\, t_j(x)\, d\Gamma(x) - \int_\Gamma T_{ij}(y,x)\, u_j(x)\, d\Gamma(x) \quad y \in S \tag{1}$$

where i and j denote Cartesian components; U_{ij} and T_{ij} represent the Flamant displacement and traction fundamental solutions, respectively, at a boundary point x. If r, denoting the distance between the points y and x, is not zero, the integrals in Eq. (1) are regular. As the internal point (also called point of resource) approaches the boundary, that is, as $y \to x'$, the distance

Communicated by S. N. Atluri, 24 April 1995

A. M. Yan, H. Nguyen-Dang
LTAS-Fracture Mechanics, University of Liège
21, Rue Ernest Solvay, B 4000 Liège, Belgium

Correspondence to: H. Nguyen-Dang

r tends to zero and, in the limit, the Flamant fundamental solution exhibits singularities. They are a strong singularity of order $1/r$ in T_{ij} and a weak singularity of order $\ln(1/r)$ in U_{ij}. Assuming continuity of the displacement at the point of boundary x', the limitation of integral equation as $y \to x'$ exists and can be written as:

$$c_{ij}(x')u_j(x') = \int_\Gamma U_{ij}(x',x)t_j(x) - \int_\Gamma T_{ij}(x',x)$$
$$u_j(x)d\Gamma(x) \quad x' \in \Gamma \tag{2}$$

where the second integral stands for the Cauchy principal-value integral; for a smooth boundary at the point x', the coefficient $c_{ij}(x')$ is given by $\delta_{ij}/2$ (δ_{ij} is the Kronecker delta). The stress boundary integral equation was first derived by Cruse (1977). In the absence of body forces, the stress components can be obtained by differentiation of Eq. (1):

$$u_{i,j}(y) = \int_\Gamma U_{ijk}(y,x)t_j(x)d\Gamma(x) - \int_\Gamma T_{ijk}(y,x)u_k(x)d\Gamma \quad y \in S \tag{3}$$

where $U_{ijk}(y) = \partial U_{ij}(y,x)/\partial y_j$, $T_{ijk}(y,x) = \partial T_{ij}(y,x)/\partial y_j$

Using Hooke's law, we obtain the stress components:

$$\sigma_{ij}(y) = \int_\Gamma D_{ijk}(y,x)t_k(x)d\Gamma(x) - \int_\Gamma S_{ijk}(y,x)u_k(x)d\Gamma(x) \quad y \in S \tag{4}$$

where

$$D_{ijk}(y,x) = \lambda U_{llk}\delta_{ij} + \mu(U_{ijk} + U_{jik})$$
$$S_{ijk}(y,x) = \lambda T_{llk}\delta_{ij} + \mu(T_{ijk} + T_{jik}) \tag{5}$$

λ, μ are constant of Hooke's law.

The integrals in Eq. (4) are regular, provided $r \neq 0$. As the resource point y approaches the boundary, that is when $y \to x'$, the distance r tends to zero, S_{ijk} exhibits a hypersingularity of the order $1/r^2$, while D_{ijk} exhibits a strong singularity of the order $1/r$. As above, if the continuity of both strains and traction at x', or continuity of derivative of displacement at x' is assumed, the limit of Eq. (4) exists when $y \to x'$. For a smooth boundary, Eq. (4) can now be written as:

$$\frac{1}{2}\sigma_{ij}(x') = \int_\Gamma D_{ijk}(x',x)t_j(x)d\Gamma(x)$$
$$-\int_\Gamma S_{ijk}(x',x)u_k(x)d\Gamma(x) \quad x' \in \Gamma \tag{6}$$

where the first and second integrals stand for the Cauchy and Hadamand principal-value integral respectively. The traction components, t_j are given out by:

$$\frac{1}{2}t_j(x') = n_i(x')\int_\Gamma D_{ijk}(x',x)t_k(x)d\Gamma(x) - n_i(x')\int_\Gamma S_{ijk}(x',x)$$
$$\cdot u_k(x)d\Gamma(x) \quad x' \in \Gamma \tag{7}$$

where n_i denotes the *ith* component of the unit outward normal to the boundary, at x'. For a plane problem, i can be 1, 2. Equations (2), (7) constitute the basis of the DBEM.

The numerical implementation of the principal-value integrals that arise in above dual boundary integral equations can be carried out by the classical method of singularity subtraction. The original improper integral is transformed into the sum of a regular integral and an integral of the singular function. The former can be easily evaluated by method of Gauss, while the latter then evaluated analytically. We use different method in the implementation of the improper integrals. To the outside boundary integral equations, normal rigid body condition is used to calculate the strong singular intergrals related to T_{ij} and coefficent c_{ij}; singularity subtraction and analytic integration used to the weak singular integrals related to U_{ij}. To the boundaries of cracks, usual rigid body condition cannot be used due to the degeneracy of lips of cracks. Fortunately, when the curved cracks are usually modelled in piece-wise flat cracks, the improper integrals can be carried out effectively by direct analytic integration. Their description and the formulas can be found in Ref. of Portela, Aliabadi and Rooke (1991).

To satisfy continuity conditions of displacement and its derivative on all nodes for the existence of principal-value integrals, the discontinue quadratic elements are used as a crack modelling strategy, see Fig. 1. Strictly, it is not necessary to use discontinue elements on the surfaces A of cracks. But it is evidently convenient to use same elements on two surfaces of cracks for data processing. At corner point and the sudden change points of applied traction, the double node technique is used.

By means of nodal collocation and integration over the boundary elements, the boundary integral equations are transformed into the linear algebraic equations. As the collocation point passes through all the nodal points, the following system of linear algebraic equations is obtained:

$$\boldsymbol{Hu} = \boldsymbol{Gt} \tag{8}$$

where the matrices $\boldsymbol{H}$ and $\boldsymbol{G}$ contain integrals of the fundamental solution T_{ij} and U_{ij} respectively in case of Eq. (2) or integrals of S_{ijk} and D_{ijk} respectively in case of Eq. (7); $\boldsymbol{t}$ and $\boldsymbol{u}$ contain boundary traction components and displacement components respectively. Separating the boundary unknowns t_i, u_i in $\boldsymbol{z}$, and the boundary condition and in $\bar{\boldsymbol{z}}$, the Eq. (8) are then rearranged:

$$\boldsymbol{Az} = \boldsymbol{B}\bar{\boldsymbol{z}} \tag{9}$$

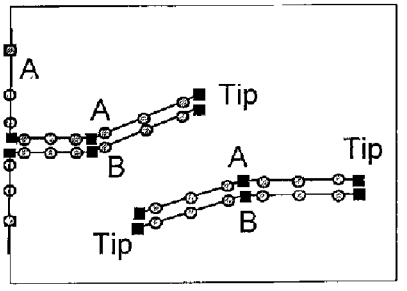

■ Element end point ⊙ Element node
A Displacement equation B Traction equation

Fig. 1. Crack modelling with discontinue quadratic boundary elements

From the system of Eq. (9), a unique solution of boundary can be obtained.

3
Stress intensity factor evaluation

The J-integral is an effective method for the determination of the stress intensity factors in present method, because the interior elastic field can be accurately determined, by using the boundary element formulae of Eqs. (1) and (4) after having obtained the solution of boundary. To each crack tip, consider a Cartesian reference system, with the origin at the tip of traction-free crack. In the absence of body forces, the path-independent J-integral is recalled here:

$$J = \oint_{\Gamma} (W n_1 - t_j u_{j,1})\, d\Gamma \tag{10}$$

where Γ is an arbitrary contour surrounding the crack tip; W is the strain energy density given out by $1/2\sigma_{ij}\varepsilon_{ij}$, where σ_{ij} and ε_{ij} are respectively stress and strain tensors; t_j are the traction components, presented by $\sigma_{ij}n_i$, where n_i are the components of the unit outward normal to the contour path. The usual relationship between the J-integral and stress intensity factors is:

$$J = \frac{K_I^2 + K_{II}^2}{\eta E} \tag{11}$$

where the constant E is the elasticity modulus; η is equal to 1 for plane stress condition and to $1/(1-\nu^2)$ for the plane strain condition, ν is Poison's ratio. A simple procedure based on the decomposition of the elastic field into its respective symmetric and antisymmetric mode components, can be used to split the stress intensity factors of a mixed-mode problem, see Kitagawa, Okamura and Ishikawa (1978). The J integral is represented by the sum of the two integrals as follows:

$$J = J^I + J^{II} \tag{12}$$

where subscript I, II is corresponding respectively to mode I and mode II of crack. Now, consider in Fig. 2 two points $P(x_1, x_2)$ and $P'(x_1, -x_2)$ symmetric to the crack line relative to the tip. The representation of (12) requires the introduction of the following decomposition in the elastic fields:

$$\begin{Bmatrix} \sigma_{11}^I \\ \sigma_{22}^I \\ \sigma_{12}^I \end{Bmatrix} = \frac{1}{2}\begin{Bmatrix} \sigma_{11} + \sigma_{11}' \\ \sigma_{22} + \sigma_{22}' \\ \sigma_{12} - \sigma_{12}' \end{Bmatrix} \quad \begin{Bmatrix} \sigma_{11}^{II} \\ \sigma_{22}^{II} \\ \sigma_{12}^{II} \end{Bmatrix} = \frac{1}{2}\begin{Bmatrix} \sigma_{11} - \sigma_{11}' \\ \sigma_{22} - \sigma_{22}' \\ \sigma_{12} - \sigma_{12}' \end{Bmatrix} \tag{13}$$

$$\begin{Bmatrix} u_1^I \\ u_2^I \end{Bmatrix} = \frac{1}{2}\begin{Bmatrix} u_1 + u_1' \\ u_2 + u_2' \end{Bmatrix}, \quad \begin{Bmatrix} u_1^{II} \\ u_2^{II} \end{Bmatrix} = \frac{1}{2}\begin{Bmatrix} u_1 - u_1' \\ u_2 + u_2' \end{Bmatrix} \tag{14}$$

It is noted that $\sigma_{ij} = \sigma_{ij}^I + \sigma_{ij}^{II}$ and $u_i = u_i^I + u_i^{II}$. Using Eqs. (13, 14) in Eq. (10), the J-integral is decomposed into two components:

$$J^m = \int_{\Gamma} (W^m n_1 - t_j^m u_{j,1}^m)\, d\Gamma \tag{15}$$

with $m \in [\mathrm{I}, \mathrm{II}]$. Finally, the relation (11) may have the alternative forms following:

$$J^I = \frac{K_I^2}{\eta E}, \quad J^{II} = \frac{K_{II}^2}{\eta E} \tag{16}$$

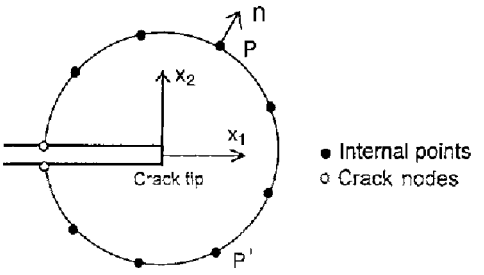

Fig. 2. Co-ordinate reference system and contour path for J-integral

In present work, the circular paths centred at the crack tip and containing a pair of crack nodes are used for each crack tip, see Fig. 2. The integration along the contour path is accomplished by means of the trapezoidal rule. The calculation with different paths shows high stability of stress intensity factors, see Yan and Nguyen-Dang (1994).

Another general and simple method for the evaluation of stress intensity factors is the near-tip displacement extrapolation. In the neighbourhood of the crack tip, the elastic field is defined by an infinite series expansion that can be decoupled into mode I and II components. Let r, θ be a polar co-ordinate system, centred at the crack tip, such that $\theta = \pm\pi$ defines the crack surfaces. Considering only the first term of the Willians' expansion, the displacement field on the crack surfaces can be written as:

$$u_2(\theta = \pi) - u_2(\theta = -\pi) = \frac{\kappa + 1}{\mu} K_I \sqrt{\frac{r}{2\pi}} \tag{17}$$

$$u_1(\theta = \pi) - u_1(\theta = -\pi) = \frac{\kappa + 1}{\mu} K_{II} \sqrt{\frac{r}{2\pi}} \tag{18}$$

where μ is the shear modulus and $\kappa = 3 - 4\eta$; for plane strain $\eta = \nu$ and for plane stress $\eta = \nu/(1+\nu)$, ν is the Poison's ratio. Using the solution of boundary at the surfaces of crack it is easy to calculate the stress intensity factors K_I and K_{II} from (17) and (18). The results of numerical tests show that this method is not very precise due to the use of discontinuous elements. But it is still useful to determine the sign of K_{II} (positive or negative) and going a step further to determine the direction of extension of crack.

4
Fatigue crack growth analysis

In present work, the analysis of fatigue crack growth is introduced as a post-processing procedure. That is, for each increment of the crack extension, the dual boundary element method is applied to carry out a stress analysis of the cracked structure and J-integral technique is used for the evaluation of the stress intensity factors while formulae (18) is used to determine the sign of K_{II}. Then, we compute the direction of the crack growth and extend at each crack tip one increment along the direction obtained by the computation. This basic computational cycle is repeatedly executed until the instability of cracked body happens ($K_{Ieq} > K_{Ic}$) or a specified number of crack-extension increment is reached. As the results of each computational step, the crack growth path, the residual

strength and fatigue-life diagrams of the cracked body can be obtained. In following discussion, a structure with multiple edge or centre cracks is considered.

In general, the path of crack growth is curved path. In the present approach it is simulated by an incremental crack extension, that is to assume a piece-wise linear discretization of crack path. For each increment analysis, crack extension is conveniently modelled with new boundary elements. In such a way, remeshing is no longer necessary. There exist already several criteria for the specification of the direction of crack growth under in-phase mixed-mode loading. The most important are: (a) maximum principal stress criterion, Erdogan and Sih (1973) (b) maximum energy release rate criterion, Hussain, Pu and Underwood (1974); and (c) strain energy density criterion, Sih (1973). Nevertheless, these criteria predict kink angles of almost the same size, especially in the case of small or medium mixed mode ratio (K_{II}/K_I). Experimental results have verified their effectiveness in most cases. In present work, the maximum principal stress criterion is applied, which postulates that the growth of the crack will occur in a direction perpendicular to the maximum principal stress. Thus, at each crack tip the local direction of crack growth θ_i is determined by the condition that the local shear stress is zero, that is:

$$K_{I_i} \sin\theta_i + K_{II_i}(3\cos\theta_i - 1) = 0 \tag{19}$$

where θ_i is the crack growth angle co-ordinate centred at i-th crack tip. The equivalent mode I stress intensity factor is defined at i-th crack tip:

$$K_{Ieq_i} = K_{I_i}\cos^3\frac{\theta_i}{2} - 3K_{II_i}\cos^2\frac{\theta_i}{2}\sin\frac{\theta_i}{2} \tag{20}$$

The fracture condition then follows from $K_{Ieq} \geqslant K_{Ic}$, in which K_{Ieq} is the maximum value of $K_{Ieq_i}(i \in [1, n]$, n is number of crack tips), K_{Ic} is the fracture toughness of the material. As a continuous criterion, crack growth angles defined by this method do not take account of the discreteness of the extension. The incremental extension of a crack in a general mixed-mode deformation field, computed by Eq. (19), is always defined locally in the same direction, whatever length of crack extension Δa is considered. As a consequence, uniqueness of the crack path cannot be assured with different sizes of the crack-extension increment. Fortunately, the computational and experimental experience shows that the crack initially grows always in such direction that mode II stress intensity factors tend to vanish. Then, the direction of crack growth may change slightly. In this case, influence of Δa is not very important. On the other hand, if the selected size of Δa is very small, some difficulties may arise in calculating the stress intensity factors after the extension. Basing on these considerations, this problem is simply dealt with in general case. First, one crack-tip having maximum value of K_{Ieq} is selected as principal crack tip. And first crack extension Δa at principal crack tip is chosen smaller (e.g. two times the length of the initial crack-tip element) than later increment (e.g. three time of length of the initial crack-tip element). The relative extensions at other crack tips, Δa_i can be simply evaluated by following proportional relation:

$$\Delta a_i = \Delta a(\Delta K_{effi}/\Delta K_{eff})^m \tag{21}$$

This relation is derived from the later Eq. (22), here m is constant of Paris' law. Then the number of boundary element increment at each crack tip is determined according to the size of Δa_i. It is obvious that the first crack extension Δa is always determined according to initial element pattern of cracks. For instance, an appropriate choice of this mesh can be determined by the relative size and geometry of cracks. In general, this simple method predicts a satisfactory result of crack growth path. For a more complex case where the direction of the service loading changes continually, or where the local symmetry at the crack tip is always upset during crack growth by the geometry of the component, the size of Δa becomes sensitive and a correcting procedure proposed by Portela, Aliabadi and Rooke (1992) should be applied to obtain more precise results.

The analysis of fatigue crack life envisages the problem of showing the relation between the number of cycles of loading and the increments of cracks to obtain the final life of the cracked structure. As the first step of the present work, the simplest loading case is considered, in which the loading cycles have a constant amplitude and may be described by a constant maximum/minimum stress ratio. For a multiple crack-tip system, one needs to carry out the life-calculation only at a principal crack tip which can be selected according to values of initial effective stress intensity factor of the crack tips. In order to show the variation in the number of loading cycles as a function of crack length, we take a generalised Paris mode defined as:

$$\frac{da}{dN} = C(\Delta K_{eff})^m \tag{22}$$

where a is the crack length at principal crack tip selected, N is the number of load cycles, C and m are material dependent constants and ΔK_{eff} is the range of the effective stress intensity factor. Here, Tanaka's model, see Tanaka (1974), is applied in mixed-mode analysis as following, since it has been verified experimentally.

$$\Delta K_{eff} = (\Delta K_I^2 + 2\Delta K_{II}^2)^{1/2} \tag{23}$$

where the stress intensity factor range of the individual modes is given by $\Delta K = K_{i\max} - K_{i\min} = K_{i\max}(1 - R)$, in which $R = K_{i\min}/K_{i\max} = \sigma_{\min}/\sigma_{\max}$ is the load ratio of the loading cycle. Thus, although the maximum principal stress criterion is used for fracture criterion and for the prediction of crack growth direction, Tanaka's model is applied in fatigue-life analysis. The number of loading cycles required to extend the crack a given increment is evaluated by integration of Eq. (22) with the trapezoidal rule.

The computational steps are illustrated by the flowchart shown in Fig. 3. A new program of dual boundary element method BECOME has been developed in our LTAS (Laboratory of Aerospace Technique). This programme can be used to analyse fatigue crack propagation of tow-dimension multiple-cracked body. In order to obtain the appropriate initial boundary elements, a parameter of ratio q is used. If $q = 1$, all elements of a line have same size; if q is greater than 1, the dimension of elements is not divided equally and on the surfaces of cracks, the ratio of discretization will be more and more

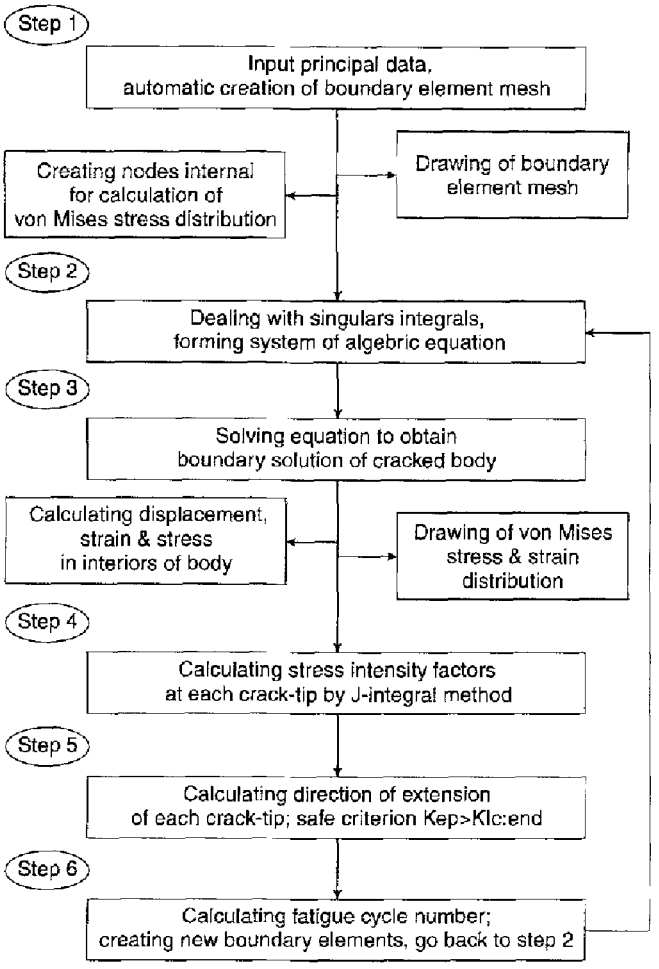

Fig. 3. Flowchart for DBEM program

small towards the tips. If the fracture toughness and Paris' constant of material is known, fatigue-life evaluation can be carried out. Otherwise, crack-extension analysis can be done with a selected crack-increment number.

5
Numerical examples

The DBEM program has been proved in various two-dimension numerical examples, see Yan and Nguyen-Dang (1994a, b). Here, all numerical examples are concerned on the problem of crack extension and fatigue life. Loading cycle is limited as a simple process of loading and unloading, that is, the minimum /maximum loading ratio $R = 0$. But, in the case of $R \neq 0$, the analyis is completely similar. As a example, a kind of aeroplane material, aluminium alloy *Al* 2024-T3, is studied when the fatigue-life analysis is included. This material has the characteristic parameter as following:

$E = 74000\ \mathrm{N/mm^2}$	(elastic modulus)
$\nu = 0.3$	(Poison's ratio)
$K_{Ic} = 1897.36\ \mathrm{N/mm^{3/2}}$	(fracture toughness)
$m = 3.32$	(Paris' exponent)
$C = 2.087136 \times 10^{-13}$	(Paris' constant)

The results of calculation are presented in the diagram of crack growth path, fatigue strength-crack increment extension and fatigue life relation.

5.1
The two collinear edge cracks in fatigue growth

A rectangular plate, with a pair of collinear edge cracks of length a, is subjected to uniform cyclic traction ($\Delta p = 100$) at the two ends. The height $2H$ is 400 and width $2W$ is 200. Initial length of each crack is 30. The 38 quadratic elements are used on external boundary, and 4 initial discontinuous elements on each surface of cracks. Figure 4 shows initial boundary element mesh and crack increment extensions.

Figure 5 presents the results in terms of crack extension and normalised stress intensity factor diagram. The comparison of present results with accurate results of Keer and Freedman (1973) shows good accuracy of present method (Δ is less than 0.6%). Figure 6 presents the extension of cracks corresponding to number of cyclic loading, as a fatigue-life diagram. The fracture-life of structure is evaluated as 6884 cycles when the cracks grow to the length of 67.2. It is justified that the II mode stress intensity factor remains zero and cracks growth in the original direction due to the symmetry of loading and geometry.

5.2
Mixed-mode cracks in fatigue growth

Now, we study the mixed mode crack problem. First, we consider a rectangular plate (200 × 100) with a slant edged

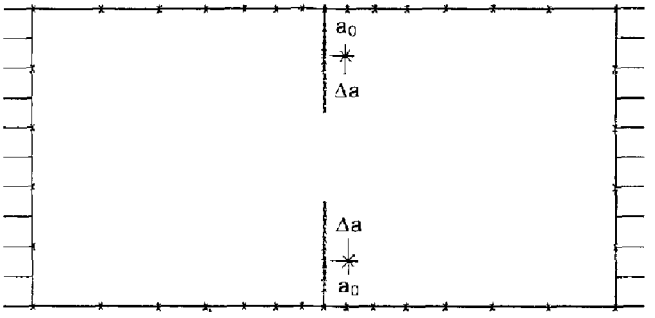

Fig. 4. Boundary element mesh and crack growth path for collinear edge cracks problem

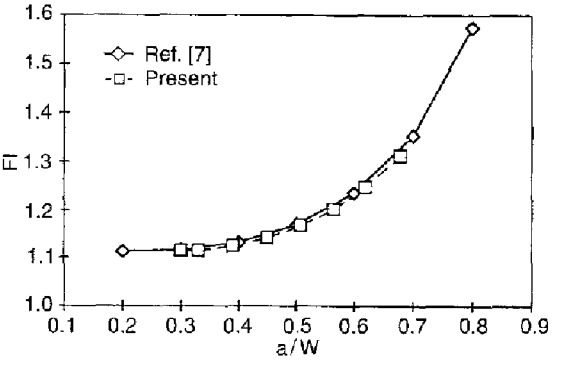

Fig. 5. Normalised stress intensity factors vary with crack growth $FI = KI/p\sqrt{(\pi a)}$

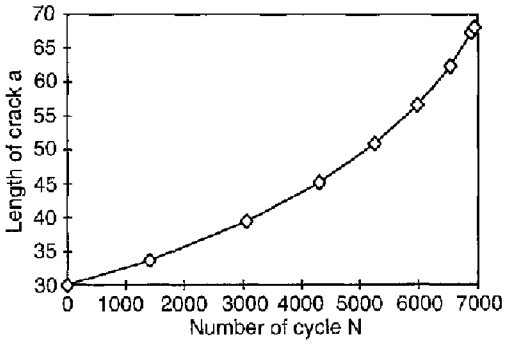

Fig. 6. Fatigue-life diagram for a pair of collinear edged crack problem

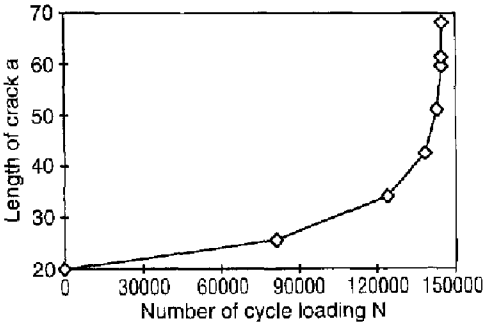

Fig. 9. Fatigue-life diagram for inclined edged crack problem

crack ($a_0 = 20$) in the angle of $-40°$ under cycle loading $\Delta p = 40$ at two ends. The 24 quadratic elements are used on external boundary, and 4 initial discontinuous elements on each surface of crack (Fig. 7). The results in term of extension of crack growth and stress intensity factors, as well as fatigue life are presented in Figs. 8 and 9 respectively. The fracture life of structure is evaluated as 144885 cycles when the crack extends to the length of 61.2, while Andre (1990), using finite element method, gives out the results corresponding as 141235 cycles for a final crack length of 61.4. These results are in good agreement.

It is noted that due to the disappearance of the initially II-mode stress intensity factor K_{II}, a sudden change of the direction of crack growth happens to form a kink angle. The reality is that the value of K_{II} tends rapidly to null and subsequent crack path is either straight or slightly curved, which is nearly perpendicular to applied load. The results of central slant crack problem (Fig. 10) is completely similar.

Now let us consider a more practical structure shown by Fig. 11. This is one fourth part of a symmetric structure with two holes. A crack is appeared on the small hole and the bigger hole sustains cyclic loading. It is interesting to point out that the crack located at boundary of small hole tends to propagate to big hole by a direct way. This situation is due to the evolution of stress field. In fact, in the radial direction of the big hole, stress field has tendency to become symmetric that leads to annul K_{II}.

5.3
Two internal no-collinear cracks in fatigue growth

As a last example, we consider a more complicated problem: a pair of no-collinear cracks having same length ($2a_0 = 10$) in

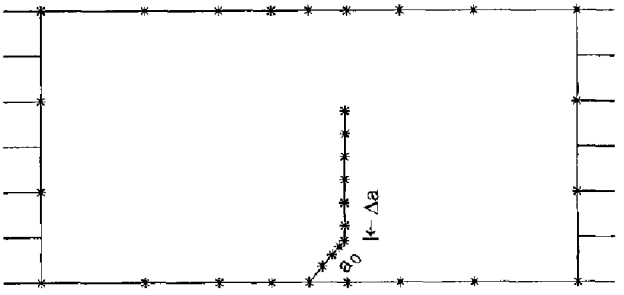

Fig. 7. Boundary element mesh and crack growth path for inclined edge crack problem

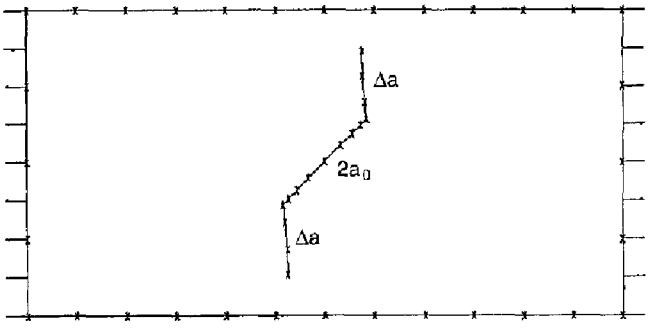

Fig. 10. Boundary element mesh and crack growth path for inclined central crack problem

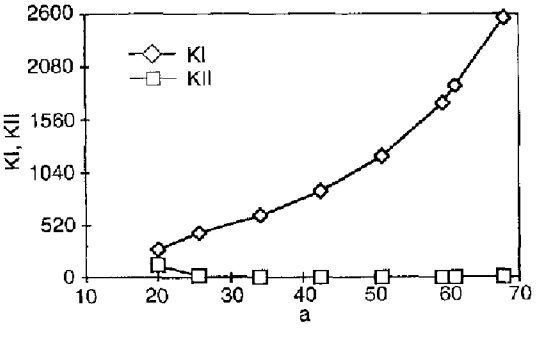

Fig. 8. Stress intensity factors vary with crack growth

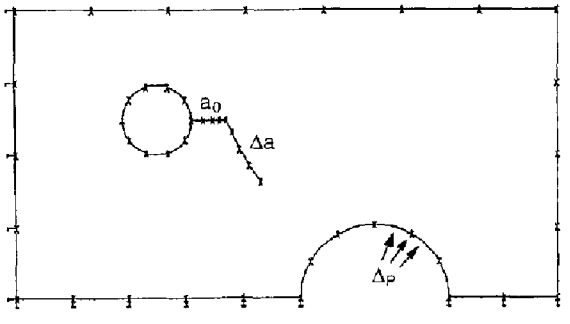

Fig. 11. Boundary element mesh and crack growth path for cracked plate with holes

interior of a rectangle (180 × 90) under fatigue loading $\Delta p = 160$ at two end (Fig. 12). The cracks are located at vertical distance of 5. The inital horizontal distance between two internal cracks tips (A) is 15. The results of Fig. 13 are given out in case of initial 44 quadratic elements in outside boundary and 6 elements at each surface of cracks.

Figure 13 shows that the intensity factors at crack tips internal (A) and external (B) are initially about same. Then, the stress intensity factors at crack tips-A, (where there are greater interaction of two cracks), increase more rapidly than at crack tips-B. But when crack tips-A are overlapped, the stress intensity factors tend afterward to decrease because of stress relaxation, while stress intensity factors increase continuously at crack tips-B. Correspondingly, crack grow more rapidly first at internal crack tip-A, finally at external crack tips-B, see Fig. 14. The prediction of crack growth path by present method is in good agreement with a experimental result in a similar structure, see Fig. 12(b), which is a real path of crack growth recorded through the surface replica of the cracks on the specimen by Tu and Cai (1993).

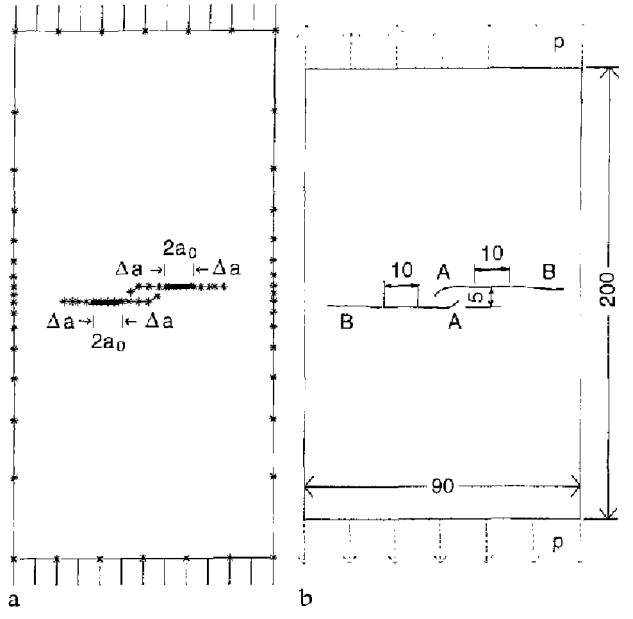

Fig. 12a, b. a Boundary element mesh and crack growth path for no-collinear central crack problem b experimental result of crack growth path through the surface replica of the cracks on the specimen

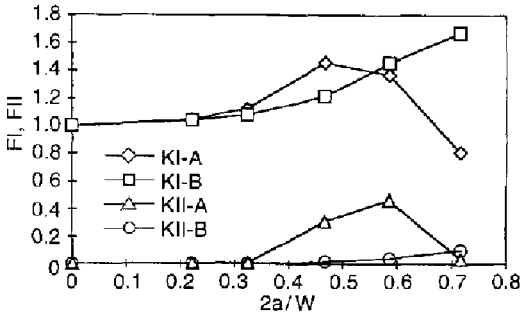

Fig. 13. Normalised stress intensity factors at each crack tip vary with crack growth $(F_I, F_{II}) = (K_I, K_{II})/p\sqrt{\pi a}$

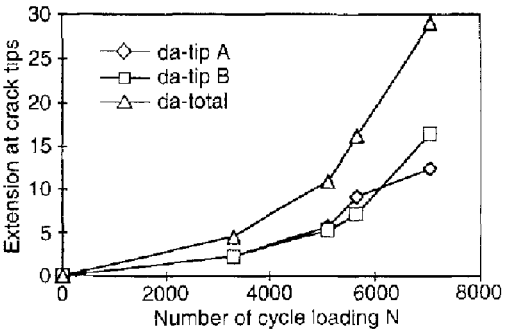

Fig. 14. Crack extension-Number of cyclic loading diagram for a pair of no-collinear central crack problem

Although the direction of service loading remains same, the cracks grow still in a curved manner because the local symmetry at the crack tips-A is upset during crack growth by the geometry of the cracked component.

6 Conclusions

Dual boundary element method is applied to the fatigue analysis of multiple-cracked body for the simple case of constant amplitude loading cycles. For each increment of the cracks, a stress analysis is carried out using DBEM and the stress intensity factors are evaluated by means of the J-integral technique. This basic computational step is repeated for every time crack extension at each crack tip. The direction of crack growth is predicted by the maximum principal stress criterion. The real curved path of crack growth is simulated by the piece-wise linear crack increments. The extension of cracks at each tip are modelled conveniently as new boundary elements. Numerical examples of various cracked geometry show high efficiency of present method. It is noted that for general fatigue crack growth under mixed mode, the cracks change abruptly their direction of growth that results in the tendency of annulling of the stress intensity factor of mode II. Kinked and subsequently straight or slightly curved cracks are taken place. However, the cracks grow in a continuously curved manner when the direction of the service loading is continually changing, or when the local symmetry at the crack tips is upset during crack growth by the geometry factor of component.

References

Andre, R. 1990: Calcul de prevision de durée de vie de pieces fissurees soumises à la fatigue, Mémoire de fin d'etude d'Ingenieur civil, University of Liège

Bueckner, H. F. 1973: Field singularities and related integral representation, Mechanics of Fracture, (ed. by Sih, G. C.), Volume 1, Nordhoff

Cruse, T. A. 1977: Mathematical foundations of the boundary integral equation method in solid mechanics, Report N°. AFOSR-TR-77-1002, Pratt and Whitney Aircraft Group

Erdogan, F.; Sih, G. C. 1963: On the crack extension in plates under plane loading and transverse shear, J. Basic Eng. 85: 519–527

Hong, H.; Chen, J. 1988: Derivations of integral equations of elasticity, Journ. Engng. Meth. 114 (6): 1028–1044

Hussain, M. A.; Pu, S. L.; Underwood, J. 1974: Strain energy release rate for a crack under combined mode I and mode II, in Fracture Analysis, ASTM STP560, ASTM, Philadelphia 2–28

Keer, L. M.; Freedman, J. M. 1973: Tensile strip with edge cracks, Int. J. Engng. Sci. 11: 1265–1275
Kitagawa, H., Okamura, H.; Ishikawa, H. 1978: Application of J-integral to mixed-mode crack problems, Trans. JSME, N°, 760–13, 46–48; ibid, N°. 780–4, 52–54
Park, J. H.; Atluri, S. N. 1993: Fatigue growth of multiple cracks near a row of fastener holes in a fuselage lap joint, Computational Mechanics 13: 189–203
Park, J. H.; Singh, R.; Chang, R. Pyo; Atluri, S. N. 1994: Structural integrity of panels with multisite fatigue damage, 35th AIAA-94-1457-CP Structure, Structure Dynamics and Material conference, 1191–1200
Portela, A., Aliabadi, M. H.; Rooke, D. P. (1991): The dual boundary element method: effective implementation for crack problem, Int. Journ. Num. Meth. Engng. 33: 1269–1287
Portela, A.; Aliabadi, M. H.; Rooke, D. P. 1992: Dual boundary element analysis of fatigue crack growth, in Advances in Boundary Element Methods for Fracture Mechanics (ed. by Aliabadi, M. H.; Brebbia, C. A.)
Sih, G. C. 1973: Some basic problems in fracture mechanics and new concepts, Journ. Engng. Frac. Mech. 5: 365–377
Tanaka, K. 1974: Fatigue crack propagation from a crack inclined to the cyclic tensile axis, Eng. Frac. Mech. 6: 493–507
Tu, S.-T.; Cai, R.-Y. 1993: A coupling of boundary elements and singular-integral equation for the solution of the fatigue cracked-body, Stress Analysis, 239–247
Watson, J. O. 1986: Hermitian cubic boundary elements for plane strain, in Developments in Boundary Element Methods 4 (ed. by Banerjee and Watson), Elsevier Applied Science Publishers, Barking, U.K.
Yan, A. M.; Nguyen-Dang, H. 1994a: Elastic analysis of the multiple-cracked structure by BEM, IIIe Congrès National de Mécanique Théorique et Appliquée, (ed. by Hogge M.; Dick E.), Comité National de Mécanique Théorique et Appliquée Belgium, 1–4
Yan, A. M.; Nguyen-Dang, H. 1994b: Stress intensity factor and crack extension of the multiple-cracked pressure cylinder, Eng. failure Analysis 1 (4): 307–315